High Ductility Aseismic Joint Spliced Pile Behavior When Subjected to Liquefaction-induced Large Ground Displacements

F. Miura[1], T. Miyasaka[2], and T. Hirata[3]

ABSTRACT

Instead of traditional welding splicer, a High Ductility Aseismic Joint (HDAJ) was newly developed for pile splicing. In order to examine the energy dissipating effect of HDAJ and pile responses to large ground displacements, the following procedures were performed. First, we conducted a series of bending experiments to elucidate the characteristics of the splicing. Then, we simulated the results of the experiments by using a nonlinear FEM which took into account both geometric and material nonlinearities to check the validity of the method. Finally, we performed numerical analyses to investigate the effectiveness of HDAJ spliced piles when subjected to liquefaction-induced large ground displacements. The numerical analyses revealed that the new pile structure would sustain ground displacements almost twice the magnitude of that sustained by ordinary piles for a given axial load.

---

1 - Professor, Yamaguchi University, Ube, Yamaguchi Pref., Japan

2 - Chief Engineer, Daido Concrete Co. LTD, Tokyo, Japan

3 - Graduate Student of Masters Course, Yamaguchi University, Ube, Yamaguchi Pref., Japan

INTRODUCTION

Earthquake damage to underground structures is classified into two categories; first, that caused by inertia and, second, that caused by permanent ground displacements. A typical example of the latter is liquefaction-induced large ground displacements. The effect of these displacements on underground structures such as buried pipes and pile foundations has been studied in the past decade. Stewart et al. (1988) and Miura et al. (1989, 1990) proposed a nonlinear finite element method to analyze the performance of piles when subjected to liquefaction-induced permanent ground displacements. The geometric and material nonlinearities of the pile and the material nonlinearity of the soil were taken into consideration in the method.

The authors also examined the performance of Prestressed High-strength Concrete (PHC) piles when subjected to large ground displacements and found that the piles would develop a plastic hinge at the interface between the liquefied layer and nonliquefied layer when the lateral displacement of the ground reached 10 to 20 cm (Miyasaka et al.1994). Meanwhile, according to field observations from the 1964 Niigata earthquake, the magnitude of lateral ground displacements was 1 m or so in highly urbanized areas, and several meters along rivers. This means that almost all piles would be broken if such lateral ground displacements took place. If a pile has higher ductility and can sustain larger lateral ground displacements, for instance 1 m or so, the safety of structures supported by pile foundations will be dramatically increased.

With this in mind, we developed a new pile structure. That is, a pile with a High Ductility Aseismic Joint (HDAJ) as pile splicing instead of the traditional welding splicer. In this paper, we first explain the mechanism and basic principle of the HDAJ. Second, the results of a series of bending experiments conducted to obtain the essential properties of piles with HDAJ are discussed. Third, the procedure for modeling the pile and ground nonlinear system and the numerical analysis method based on the FEM are explained. After checking the validity of the numerical analysis method by simulating the experiment results, we investigate the pile responses to liquefaction-induced permanent ground displacements, and discuss the effectiveness of HDAJ spliced piles.

HIGH DUCTILITY ASEISMIC JOINT

(1) Basic structure

The basic structure of the HDAJ is shown in Figure 1. In this joint structure, three main components are provided: pile tip fittings with circumferential grooves which are connected to the end of upper and lower piles, a circumferentially multi-divided cylindrical inner ring, and a

cylindrical outer ring. The joint is assembled by first setting the upper pile vertically onto the lower pile, then engaging the inner rings on the grooves of the tip fittings, and finally pushing the outer ring longitudinally upward. Both the outside surfaces of the inner ring and the inside surface of the outer ring have conical tapers. Since the taper directions are opposite, pushing the outer ring upward results in a firm coupling of the piles.

(2) Bending characteristics

We performed a series of bending experiments on piles with and without HDAJ. A schematical diagram of the specimen and the observation points is shown in Figure 2. The length of the span is 7.2 m. The angle of rotation, θ (4 points), strain, ε (4 points), and deflection, δ (5 points), were observed as shown in the figure. Table 1 summarizes the conditions of the four test cases used in the experiment. All the tested piles were PHC piles with outer diameters of 400 mm.

The test results are shown in Figures 3(a) and (b). Figure 3(a) compares the results from Cases 1 and 2, i.e., the cases with zero axial load and Figure 3(b) the results from Cases 3 and 4, i.e., the cases with an axial load of 60 tf. This magnitude of 60 tf corresponds to two thirds of the allowable design bearing capacity. Arrows in these figures designate the ultimate bending moment for each case. These values and corresponding rotational angles are listed in Table 2. The values given in Table 2 are for a pile length of 0.5 m, corresponding to the length of the beam element used to model piles in the following numerical analyses. From these figures and Table 2, we can see that piles with HDAJ have ultimate rotational angles three to four times larger than those without HDAJ. In other words, HDAJ provides piles with higher ductility.

NUMERICAL SIMULATION OF BENDING EXPERIMENTS

(1) Analysis method

a) Model for analyses

Figure 4 illustrates the model for the numerical analyses. A pile is modeled by arranging beam elements and Rotational Spring-Slider Elements (RSSE) one after the other in order to express the geometric and material nonlinearity of the pile. The stiffness matrix of the beam element is given as:

$$\begin{bmatrix} \frac{EA}{l} & 0 & 0 & -\frac{EA}{l} & 0 & 0 \\ & \frac{12EI}{l^3}+\frac{6P}{5l} & \frac{6EI}{l^2}+\frac{P}{10} & 0 & -\left(\frac{12EI}{l^3}+\frac{6P}{5l}\right) & \frac{6EI}{l^2}+\frac{P}{10} \\ & & \frac{4EI}{l}+\frac{2PL}{15} & 0 & -\left(\frac{6EI}{l^2}+\frac{P}{10}\right) & \frac{2EI}{l}-\frac{Pl}{30} \\ & & & \frac{EA}{l} & 0 & 0 \\ & \text{symm.} & & & \frac{12EI}{l^3}+\frac{6P}{5l} & -\left(\frac{6EI}{l^2}+\frac{P}{10}\right) \\ & & & & & \frac{4EI}{l}+\frac{2PL}{15} \end{bmatrix} \quad (1)$$

in which l is the length of the element, E is Young's modulus, A is the area of the section, I is the moment of inertia, and P is the axial load. This stiffness matrix is a function of P, and this makes it possible to express the so called P-Δ effect. When P is equal to zero, this stiffness matrix is equal to the ordinary linear stiffness matrix of small deflection problems.

The coordinates of the nodal points of the beam elements and therefore the stiffness matrices of the elements are updated at each iteration for each load step. By virtue of the update and iteration, geometric nonlinearity of the pile is realized. The material nonlinearity of the pile is expressed by the RSSE. The usage of the element, with the exception of the relationships between the bending moment and rotational angle, is explained in detail by Stewart et al. (1988) and Miura et al. (1989, 1990). In this study, the relationships between the bending moment and rotational angle obtained from the experiments, shown in Figure 3, are used although bi-linear or tri-linear approximations for the relationships were used in the references. The values used in the analyses for Young's modulus are summarized in Table 3. These values are obtained from the experimental bending moment-rotational angle curves below the cracking moment level. It should be noted that the values from Cases 3 and 4, in which axial load exists, are larger than those from Cases 1 and 2 in which no axial load exists.

(2) Results

Figures 5(a) and (b) compare the load-deflection curves obtained from the experiments and the numerical simulations. Figure (a) compares the results from Cases 1 and 2, and (b) from Cases 3 and 4. Solid lines show the results from the experiments and broken lines from the numerical simulations. These figures show good agreement between the experimental results and the simulation results at all times. This verifies the validity of the simulation method which we employed.

PILE PERFORMANCE WHEN SUBJECTED TO LIQUEFACTION-INDUCED LATERAL GROUND DISPLACEMENTS

(1) Analysis method

a) Modeling of pile

In this study, four cases are analyzed as listed in Table 4. In all four cases, an axial load of 60 tf is assumed. Two kinds of piles are analyzed; piles without HDAJ and piles with HDAJ. For each kind, two pile cap connectivity conditions are assumed. One is a "free-end condition" , a model of which is shown in Figure 6(a). Nodal point "a" has three degrees-of-freedom, i.e., horizontal, vertical and rotational. The other is a "fixed-end condition", a model of which is shown in Figure 6(b). Nodal point "a" has two degrees-of-freedom, i.e., horizontal and

vertical. Rotational movement is fixed. An RSSE is inserted between nodal points "a" and "b". Nodal points "a" and "b" move in the same way until the bending moment of this RSSE reaches the cracking moment of the pile. In this study, the nonlinear characteristics of the RSSE at the pile cap are set to be equal to those of piles. Therefore, a plastic hinge develops here when the bending moment at the pile cap reaches the ultimate bending moment of the pile. The actual situation of pile cap connectivity lies in between the free-end condition and fixed-end condition.

b) Modeling of ground

We assumed a three-layer system for the ground model, the surface nonliquefiable layer, the middle liquefiable layer and the basal nonliquefiable layer as shown in Figure 7. The surface layer slides as a coherent mass atop the underlying liquefiable layer. In the liquefiable layer, the lateral movements are distributed linearly from the base to the top of the deposit. Shear distortion in the liquefiable soil combined with horizontal translation of the upper nonliquefiable layer results in the trapezoidal distribution of horizontal movements shown in Figure 7, which was used to model displacements in this study. We assumed a bi-linear relationship for the force-displacement relationship of pile-soil interaction as in our previous works.

(2) Analysis results

a) Free-end connectivity

Figures 8(a) and (b) show the change in distribution of pile displacements when the amplitude of ground displacement was incrementally increased from zero to 100 cm. Figure (a) shows the results from Case Pfr and (b) from Case Jfr. Both figures seem to show very similar tendencies. When the magnitude of ground displacement was very small a plastic hinge developed at the lower boundary between the basal nonliquefiable layer and liquefiable layer, but not at the upper boundary between the surface nonliquefiable layer and liquefiable layer. Judging from these figures, the effect of HDAJ seems to be negligible. However, there is a significant difference between these two cases.

In order to make clear the difference, Figures 9(a) and (b) depict the relationship between the bending moments and ground displacements. Arrows in these figures designate the ground displacements at which the bending moment induced in the pile at the lower boundary reached their ultimate values. In Case Jfr the value is almost twice as large as that in Case Pfr. On the other hand, the difference in the responses at the upper boundary is negligible.

b) Fixed-end connectivity

Figures 10(a) and (b) show the change in pile deformation as ground displacement increases as shown in Figure 8. Figure (a) is from Case Pfx and (b) from Case Jfx. The piles are almost

vertical in the surface nonliquefiable layer and large curvature exists just above the upper boundary in Case Pfx and at the boundary in Case Jfx. There is a small difference in the actual location of maximum curvature in Cases Pfx and Jfx, however, the general tendencies are very similar and a plastic hinge developed at the upper boundary in each case. Comparing Figures 10(a) and (b) with Figures 8(a) and (b) respectively, we can identify the differences between them, particularly at the upper boundary where no plastic hinge developed in Cases Pfr and Jfr.

Figures 11(a) and (b) show the bending moment-ground displacement relation curves at the locations where plastic hinges developed in Cases Pfx and Jfx. Arrows in these figures again designate the magnitude of ground displacement at which a plastic hinge developed. The ground displacements in Case Jfx are much larger than those in Case Pfx, which demonstrates the effectiveness of HDAJ.

Finally, Table 5 summarizes the ground displacements at which plastic hinges developed in all cases. These results indicate that piles with HDAJ will sustain ground displacement of almost twice the magnitude of that sustained by piles without HDAJ for a given axial load.

CONCLUDING REMARKS

A new pile structure, a pile spliced with a high ductility aseismic joint instead of traditional welding splicer, was developed. The bending characteristics of the pile were obtained by a series of bending experiments. After checking the validity of the numerical analysis method which we employed, we investigated the responses of the new pile structure to liquefaction-induced large ground displacements. From the numerical analyses, we found that the piles with HDAJ could sustain ground displacements of almost twice the magnitude as that sustained by piles without HDAJ for a given axial load. The numerical results imply the effectiveness of HDAJ, however, the number of models and conditions in this study were limited, we need further analyses to obtain more general conclusions.

ACKNOWLEDGEMENT

Finally we would like to express our sincere thanks to Professor M.Hamada of Waseda University and Mr. Y.Itoh of Daido Concrete Co. LTD for valuable suggestions and information on pile damage caused by past earthquakes. Thanks are extended to Professor T.D.O'Rourke of Cornell University and Dr. W.D.Meyersohn, former graduate student of Cornell University, for providing information on the newest version of computer code "B-STRUCT".

REFERENCES

H.E. Stewart, F. Miura, and T.D. O'Rourke: Pile damage due to large ground displacement, Proc. of the first Japan-U.S. workshop on liquefaction, large ground deformation and their effects on lifeline facilities, pp.99-126, 1988.

F. Miura, H.E. Stewart, and T.D.O'Rourke: Lateral spreading effects on pile foundations, Proc. of the second U.S.-Japan workshop on liquefaction, large ground deformation and their effects on lifeline facilities, pp.295-307, 1989.

F. Miura and T.D.O'Rourke: nonlinear analyses of piles subjected to liquefaction-induced large ground deformation, Proc. of the third Japan-U.S. workshop on earthquake resistant desing of lifeline facilities and countermeasures for soil liquefaction, pp.497-512, 1990.

T. Miyasaka, F. Miura, and J. Kiyono: Effects of P-Δ and connectivity on the nonliner response of piles subjected to liquefaction-induced large ground displacements, Proc. of the second international conference on earthquake resistant construction and design, Berling, pp.413-420, 1994.

Table 1 Test cases

	Pile length (m)	Span (m)	Axial load (tf)	HDAJ
Case 1	12.0	7.2	0.0	Without
Case 2	12.0	7.2	0.0	With
Case 3	8.0	7.2	60.0	Without
Case 4	8.0	7.2	60.0	With

Table 2 The ultimate bending moments and corresponding ultimate rotational angle

	The ultimate bending moment (tf-m)	The ultimate rotational angle (° /0.5m)
Case 1	19.8	0.733
Case 2	19.8	2.263
Case 3	27.4	0.343
Case 4	27.4	2.423

Table 3 Young's modulus used in the analyses (kg/cm^2)

Case 1	3.5×10^6
Case 2	3.5×10^6
Case 3	4.2×10^6
Case 4	4.2×10^6

Table 4 Analysis cases

	HDAJ	Pile cap connectivity
Case Pfr	Without	Free-end
Case Jfr	With	Free-end
Case Pfx	Without	Fixed-end
Case Jfx	With	Fixed-end

Table 5 Ground displacements at which plastic hinges developed

	Position of the hinge from the pile cap (m)	Ground displacement at the surface (cm)	Ratio
Case Pfr	8.5	20.4 ①	
Case Jfr	8.5	43.7 ②	②／①＝2.14
Case Pfx	8.5 2.5	17.2 ③ 31.4 ④	
Case Jfx	8.5 3.0	37.3 ⑤ 56.4 ⑥	⑤／③＝2.17 ⑥／④＝1.80

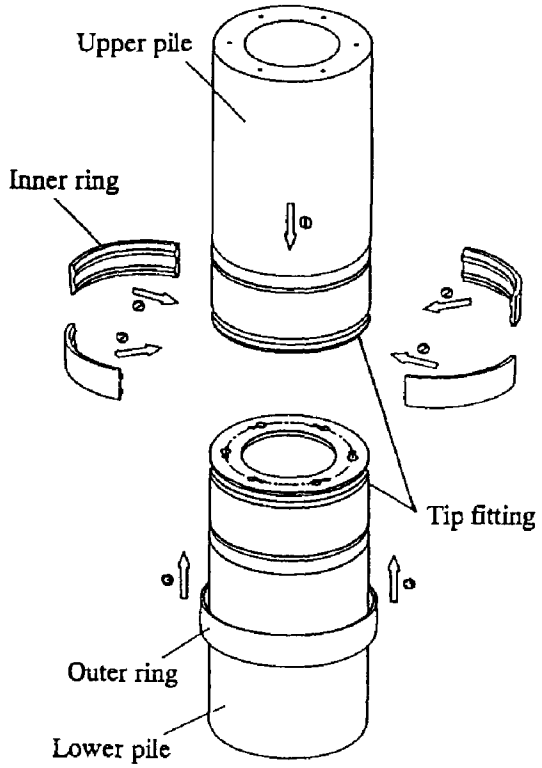

Figure 1 High ductility aseismic joint

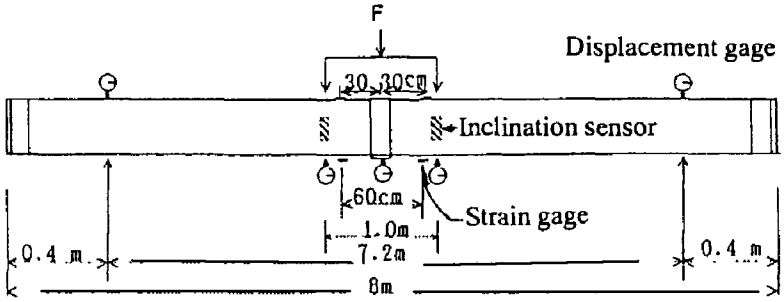

Figure 2 Schematic diagram of bending test

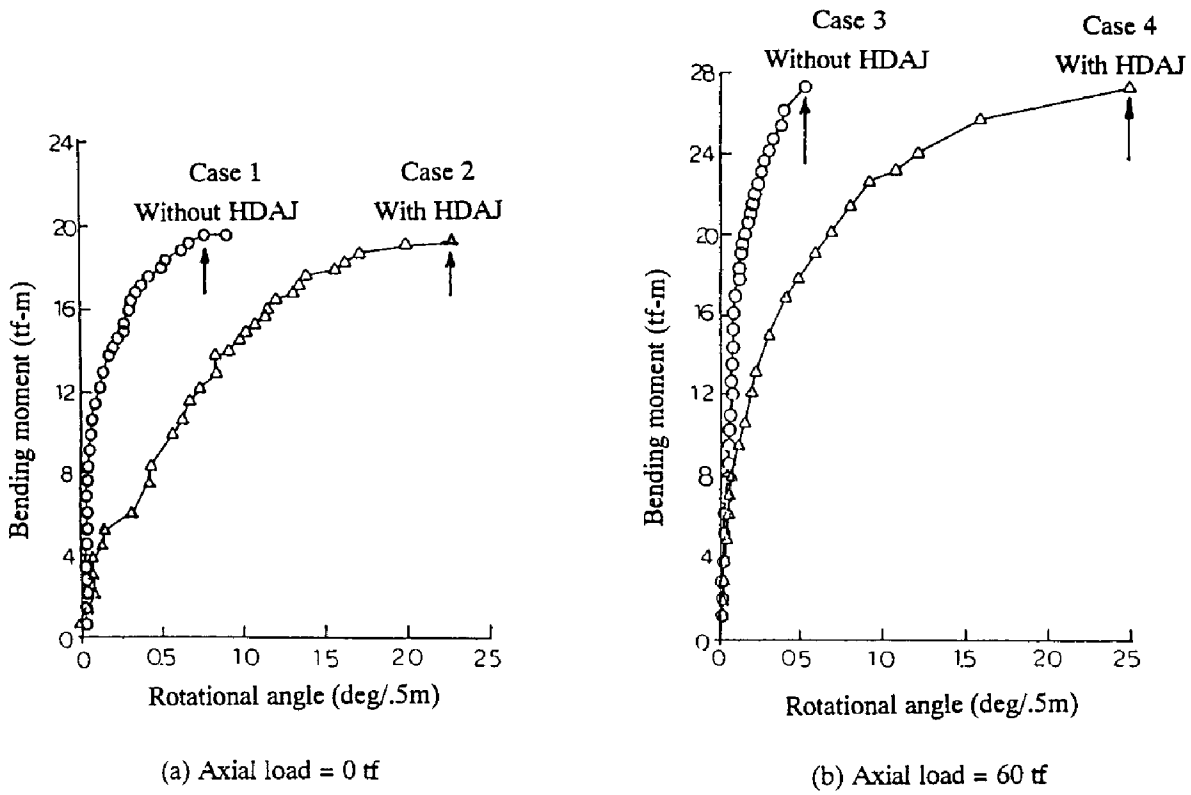

(a) Axial load = 0 tf

(b) Axial load = 60 tf

Figure 3 Resulting bending moment-rotational angle curves

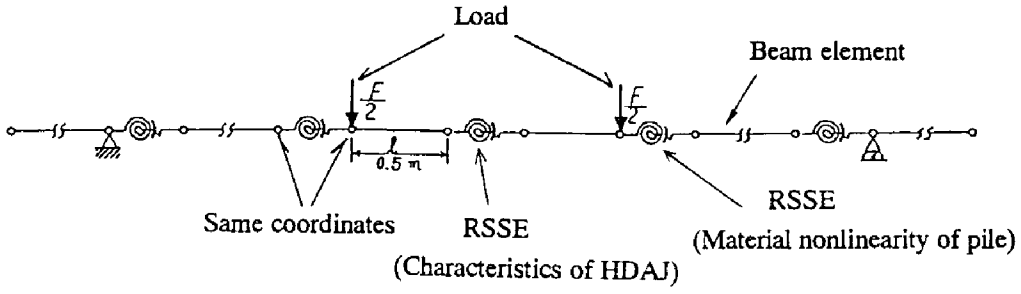

Figure 4 Pile model for numerical simulation

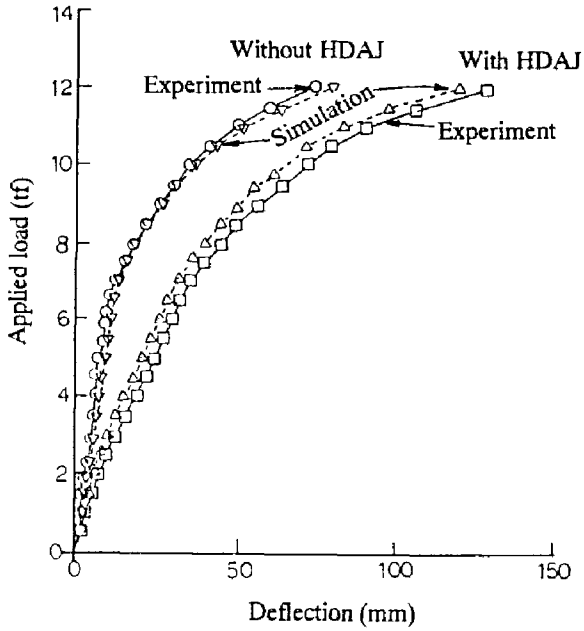

(a) Axial load = 0 tf

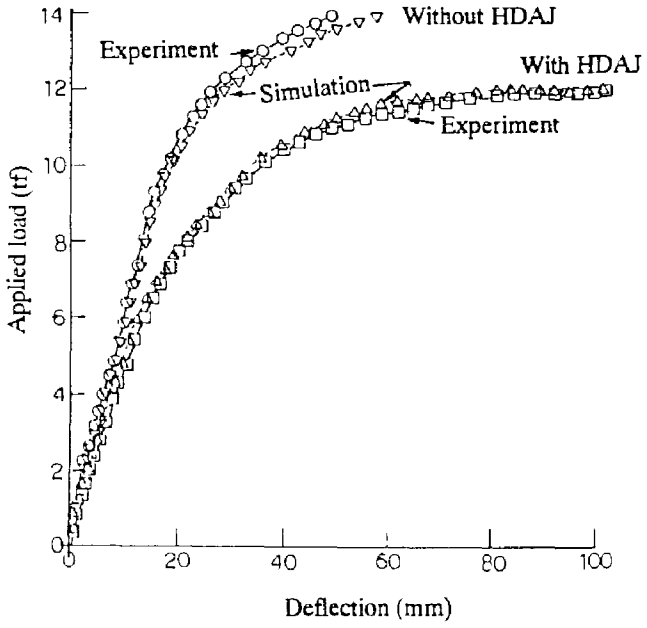

(b) Axial load = 60 tf

Figure 5 Comparison of load-deflection curves obtained from simulations with those from experiments

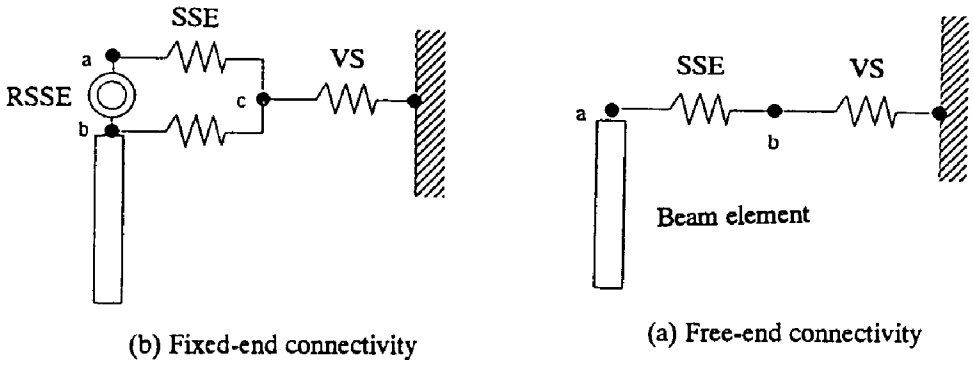

(b) Fixed-end connectivity

(a) Free-end connectivity

Figure 6 Model of pile cap

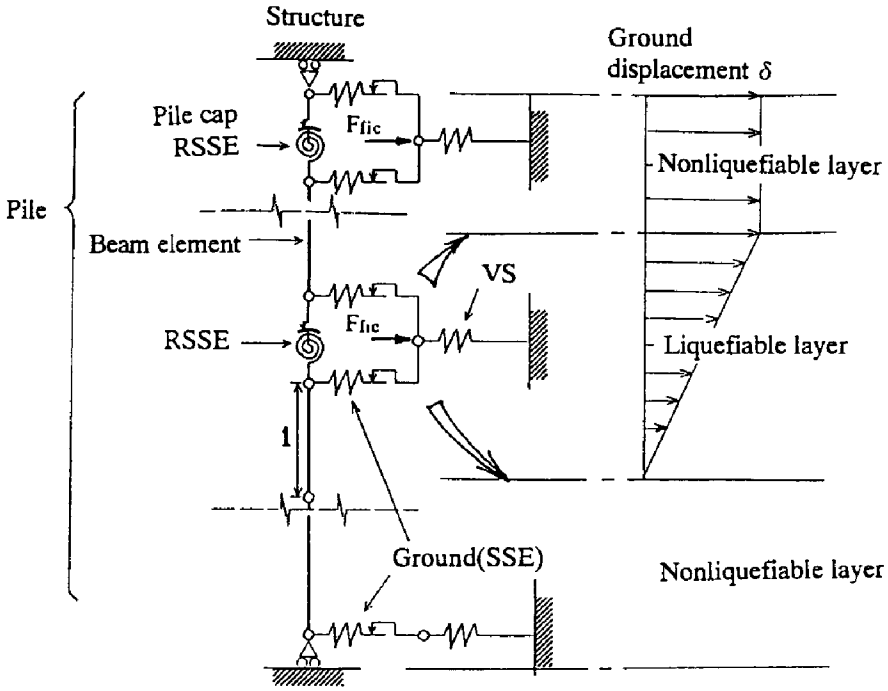

Figure 7 Model of pile and soil interaction for numerical simulation

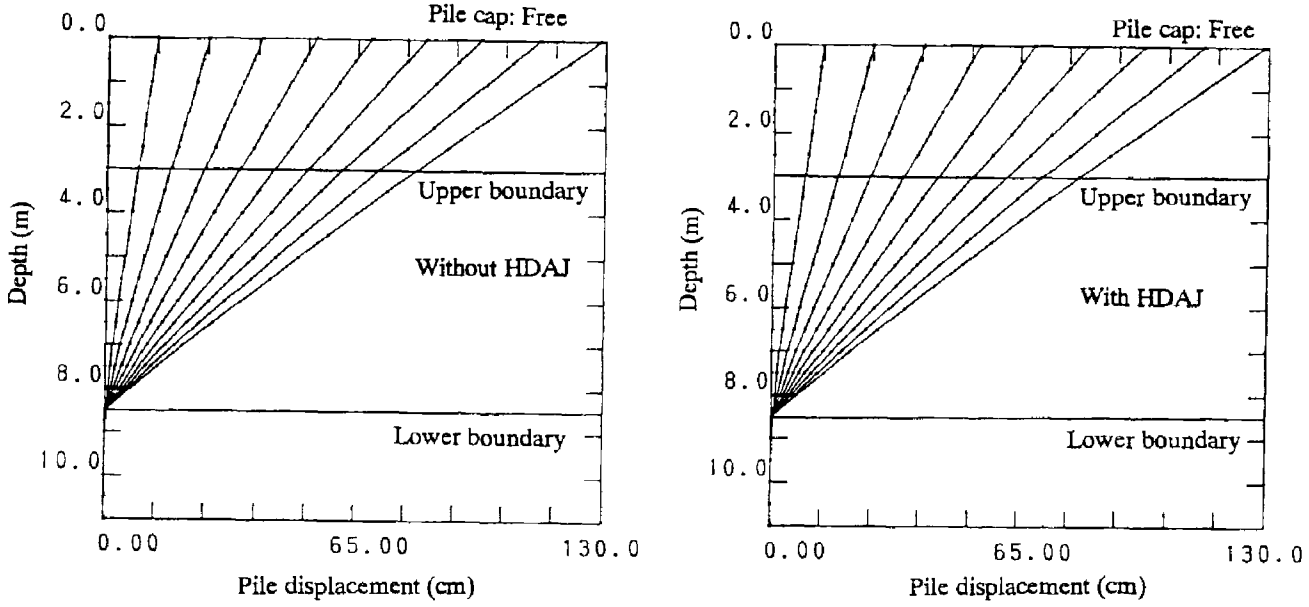

(a) Pile without HDAJ (Case Pfr)

(b) Pile with HDAJ (Case Jfr)

Figure 8 Change of pile displacement with increasing ground displacement (free-end)

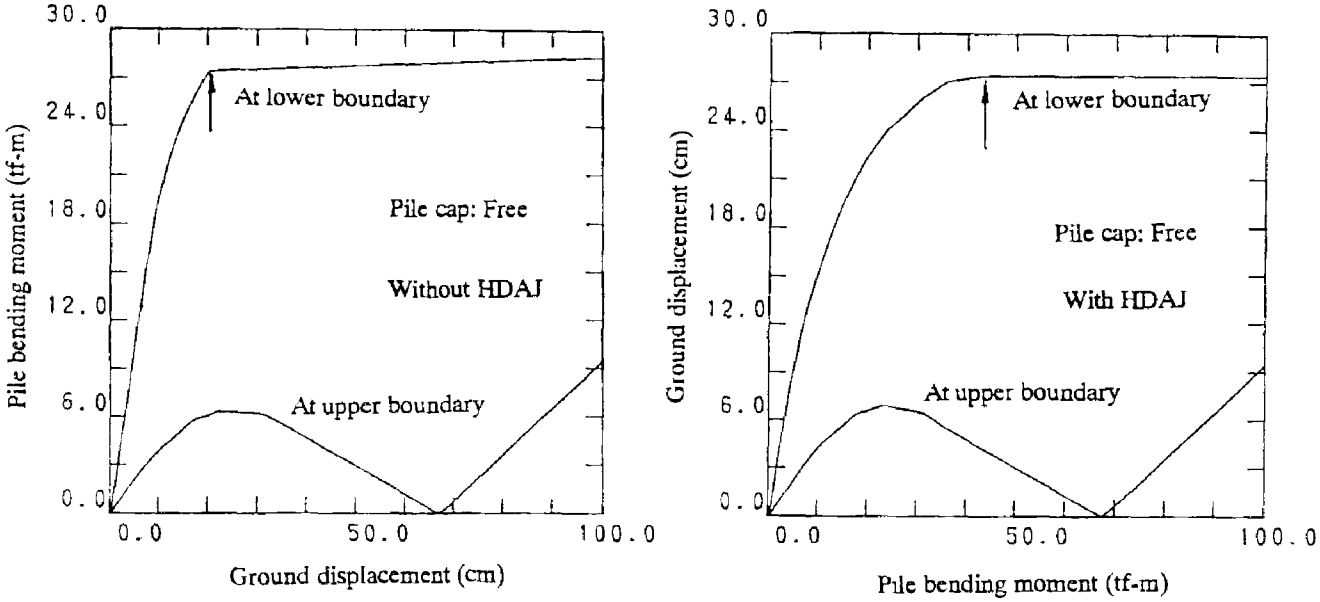

(a) Pile without HDAJ (Case Pfr)

(b) Pile with HDAJ (Case Jfr)

Figure 9 Bending moment-ground displacement curves (free-end)

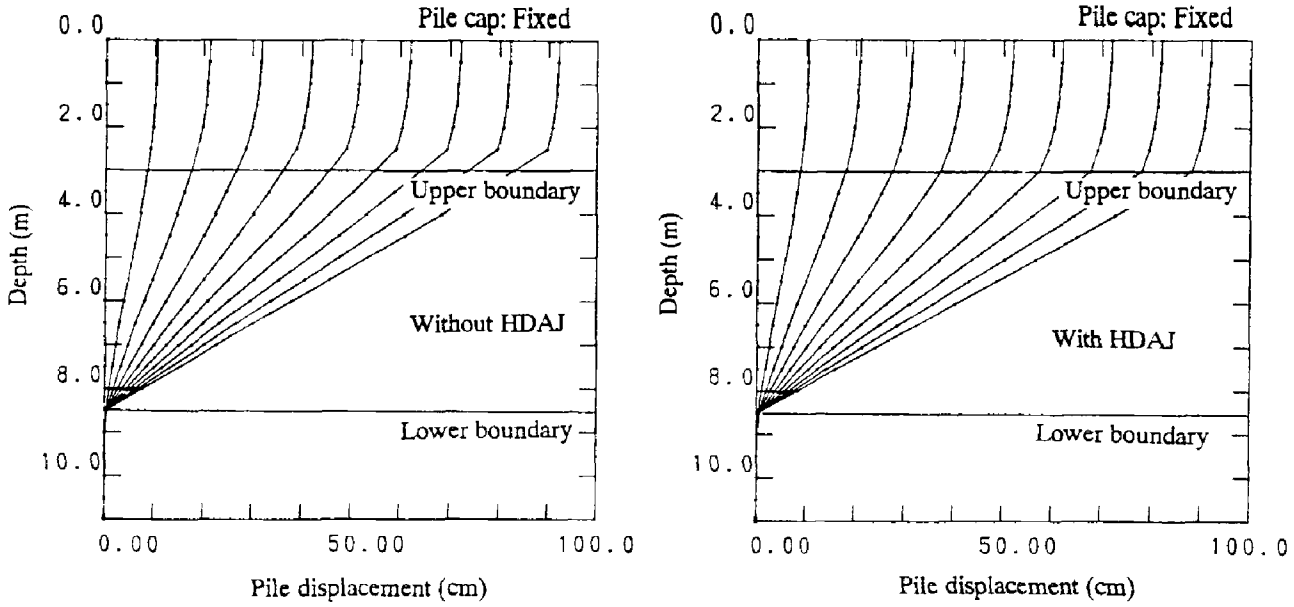

(a) Pile without HDAJ (Case Pfx)

(b) Pile with HDAJ (Case Jfx)

Figure 10 Change of pile displacement with increasing ground displacement (fixed-end)

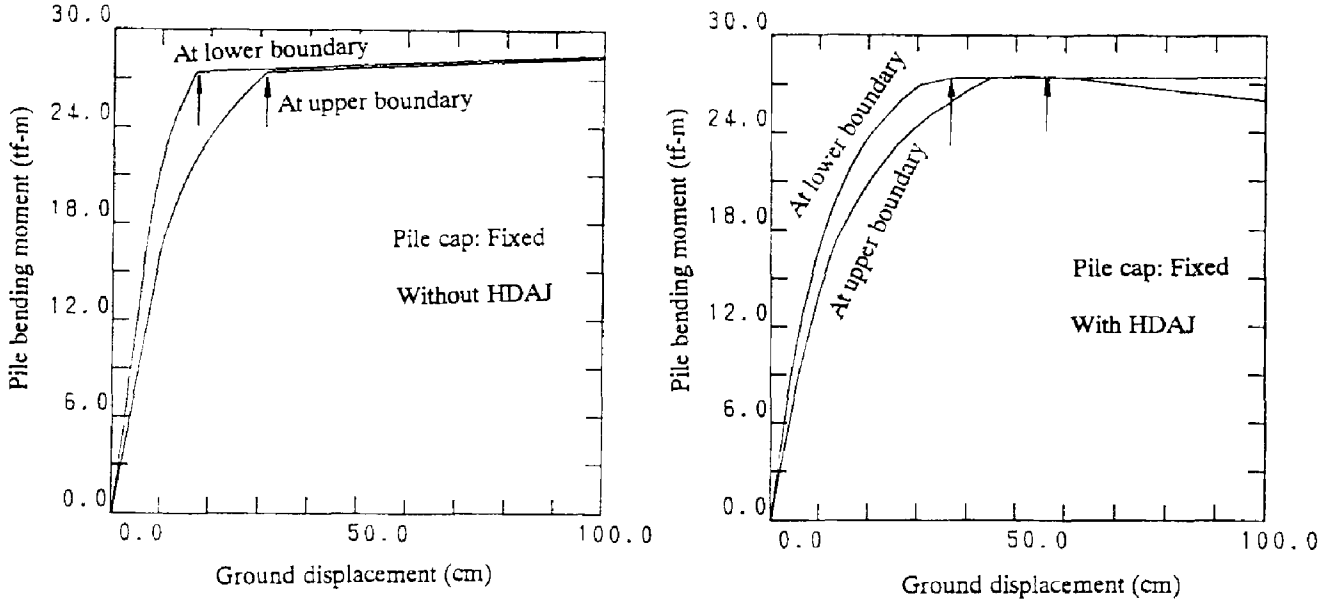

(a) Pile without HDAJ (Case Pfx)

(b) Pile with HDAJ (Case Jfx)

Figure 11 Bending moment-ground displacement curves (fixed-end)